Observing transient melting in a nanocrystal using an X-ray laser

J. N. Clark[1,8], L. Beitra[1], G. Xiong[1], A. Higginbotham[2], D. M. Fritz[3], H. T. Lemke[3], D. Zhu[3], M. Chollet[3], G. J. Williams[3], M. Messerschmidt[3], B. Abbey[4], R. J. Harder[5], A. M. Korsunsky[6,7], J. S. Wark[2] & I. K. Robinson[1,7]

[1]*London Centre for Nanotechnology, University College, London WC1E 6BT, UK*

[2]*Department of Physics, Clarendon Laboratory, University of Oxford, Parks Road, Oxford OX1 3PU, UK*

[3]*Linac Coherent Light Source, SLAC National Accelerator Laboratory, 2575 Sand Hill Road, Menlo Park, California 94025, USA*

[4]*ARC Centre of Excellence for Coherent X-ray Science, Department of Physics, La Trobe University, Bundoora, Victoria 3086, Australia*

[5]*Advanced Photon Source, Argonne, IL 60439, USA*

[6]*Department of Engineering Science, University of Oxford, Parks Road, Oxford OX1 3PJ, UK*

[7]*Research Complex at Harwell, Didcot, Oxfordshire OX11 0DE, UK*

[8]*Stanford PULSE Institute, SLAC National Accelerator Laboratory, 2575 Sand Hill Road, Menlo Park, California 94025, USA*

There is a fundamental interest in studying photoinduced dynamics in nano-particles and -structures as it provides insight into their mechanical and thermal properties out of equilibrium and during phase transitions. Nano-particles can display significantly different proper-

ties than the bulk [1] which is due to the interplay between their size, morphology, crystallinity, defect concentration and surface properties. Particularly interesting scenarios arise when nanoparticles undergo phase transitions, such as melting induced by an optical laser. Current theoretical [2] evidence suggests that nanoparticles can undergo reversible non-homogenous melting with the formation of core-shell structure consisting of a liquid outer layer. To date, studies [3–6] from ensembles of nanoparticles have tentatively suggested that such mechanisms are present. Here we demonstrate imaging transient melting and subsequent softening of the acoustic phonon modes of an individual gold nanocrystal using an X-ray free electron laser. The results demonstrate that the transient melting is reversible and non-homogenous, consistent with a 'core-shell' model of melting. The results have implications for understanding transient process in nanoparticles and determining their elastic properties as they undergo phase transitions.

Transient processes in nanoparticles are of great interest as they can provide insight into fundamental photon, electron and lattice interactions. For example, by observing the transient reflectivity of nano particle ensembles after irradiation with an optical laser in a 'pump-probe' experiment, the forces from the subsequent hot electron gas can be observed [7]. Nanoparticles also display interesting properties due to their size and morphology, for example they can display anomalously low thermal conductivity due to the phonon mean free path approaching the size of the particle which has significant implications for novel thermoelectric devices [8]. Further interest in transient process in nano particles comes from their role in photo-acoustic imaging [9], photo-thermal cancer therapy [10] and potential in high-harmonic generation [11]. Therefore, it is critical

from both a fundamental and practical point to understand irradiation of nano-particles with a short pulse ($<$100 fs) laser up to the point of melting.

Previous experimental [3,4,6] investigations of nanoparticles using 'pump-probe' experiments has eluded to partial melting of the nanoparticles with the possibility of it occurring at much lower temperatures than that of the bulk [4]. It has been claimed that the formation of a liquid outer shell begins to occur at temperatures as low as 70% of the melting temperature and within 100 ps of irradiation [4]. It has also been suggested that nanoparticles held at low temperatures (100° c) facilitate surface pre-melting [5]. The formation of liquid outer-shell is something that has been observed in static experiments [12] but has yet to be confirmed on a picosecond timescale. Simply observing the change in oscillation period during an optical pump-probe experiment of nanoparticles that have a liquid-outer shell is not expected to yield a conclusive result to its existence, as a liquid shell 20% of the radius of the nanoparticle will result in only a 3% change in oscillation period [3]. It is speculated that for temperatures below the melting temperature, the process of liquid-shell formation is reversible [2,4,12] but is still largely unconfirmed and the degree of reversibility is still an open question. Consequently, resolving the mechanisms requires imaging individual nano particles with anatomically sensitive probe such as X-rays or electrons.

Molecular dynamics (MD) simulations have provided the most detailed description of the nanoparticles response to laser irradiation at low intensity with reversible non-homogenous surface pre-melting predicted [2,13] which would consist of regions on the nano particle surface beginning to melt before producing a continuous layer. Additionally, these simulations have found that prior to

the formation of a non-homogenous liquid outer layer surrounding a solid inner core, preferential facet pre-melting can occur with liquid-like atoms appearing first in the (100) and (110) crystallographic directions. It was also observed that during the formation of the liquid outer-layer, liquid regions extended inward to the solid core. Simulations on larger nanorods [14] have suggested more exotic behavior during laser-induced pre-melting, such as internal structural changes from face-centered cubic to hexagonal close packed structures along with the formation of surface defects. Dislocation cores were found to nucleate on the crystal surface with stacking faults forming and propagating towards the interior. An important result found in the simulations was surface pre-melting arising before the formation of defects. This suggests that surface pre-melting can initiate without the formation of defects acting as surface nucleation sites.

By using spatially and temporally coherent X-ray pulses from an XFEL, coherent diffraction patterns can be recorded from individual nanocrystals due to the high number of photons per pulse. Non-equilibrium dynamics can be investigated [15] by perturbing the nanocrystal with an optical pulse, causing time dependent deformation through electron-phonon and phonon-phonon coupling. Varying the delay time between the optical perturbation and X-ray probe provides time resolved diffraction intensity. Recording the diffraction at at least twice the Nyquist frequency allows the diffraction fringes to be resolved and permits direct access to real-space information from the nanocrystal through its auto-correlation (obtained by inverse Fourier transform of the intensity) or electron density (by using iterative phase retrieval [15,16]) as a function of delay time. Additionally, by taking the Fourier transform (with respect to time) of the intensity provides direct access to the phonon dispersion [17] which can then be used to obtain materials properties such as the elastic

constants. The strength of this technique is that the phonon dispersion (and material properties) can be accessed for individual nanocrystals or structures.

The experiment was carried out using the X-ray Pump Probe instrument at the Linac Coherent Light Source (LCLS) [18] at the SLAC National Laboratory and schematic can be seen in Supplementary Fig. 1.100 fs (full-width, half duration,(FWHD)), 9.2 KeV X-ray pulses (120 Hz) were monochromatized by a silicon monochromator before being focussed by beryllium refractive lenses (see Experiment). The sample consisted of gold nanocrystals (see Methods) on a silicon nitride membrane mounted vertically and normal to both the optical pump and X-ray probe pulses. Coherent diffraction patterns were recorded using a Cornell-SLAC pixel array detector (CS-PAD)[19] placed 1.2 m from the sample at the gold (111) Brag peak. Transient melting was induced by 'pumping' the sample with a 800 nm, 50 fs (FWHD) laser using fluences of 1-2 mJ.cm^{-2}. The delay between the pump and probe pulse was used to provide the time resolved data.

Shown in Fig. 1 (a) are selected 2D data collected from the same individual nanocrystal as a function of delay time (horizontally) and pump fluence (vertically). At the lowest fluence (1 mJ.cm^{-2}), small peak shifts and some broadening are evident as the delay time changes. For small perturbations, the peak shift can be interpreted as homogenous strain (expansion and contraction of the lattice) while the distortion can be interpreted as inhomogeneous strain. The diffraction pattern becomes significantly distorted (particularly at +50 ps) for the highest fluence (SI movie 1) and has shifted considerably while becoming elongated and broad in the direction of the scattering vector. The larger shift can be broadly interpreted as in increase in average lattice temperature

(compared to the lower fluences) while the broadening of the peak may no longer be simply due to inhomogenous strain but also be due to a morphology (size) change of the nanocrystal [20], that is, the crystal is transiently melted.

The oscillatory component of the data can be seen in Fig. 1 (b), which shows the diffraction parallel to the (111) scattering vector as a function of delay time for the three fluences at different $r_{\perp}$ scattering values. The distortion at the highest fluence manifests itself (in addition to broadening) as a loss of intensity and departure from harmonic motion (which is evident in the lower fluences), something that is consistent with a picture of the nanocrystal undergoing transient melting and re-crystallization.

A linear increase in pump fluence should produce a commensurate linear increase in the lattice spacing (and peak shift) [21]. To examine the linearity of the shift in our data, the center of mass of each diffraction peak is plotted in Fig. 2 (a) as a function of fluence. This plot illustrates the harmonic motion and subsequent departure from this at the highest fluence. The peak shift, which can be directly related to a rise in lattice temperature, should be linear with fluence, however it is evident that the shift plateaus. The temperature difference during the oscillation obtained from the peak shift is 250 K. The non-linear peak shift as a function of fluence is shown in Fig. 2d which plots the peak shift for selected times. The non-linearity is also evident in the peak width, which is shown in Fig. 2e and plotted as a function of fluence for select times in Fig. 2f. As mentioned earlier, the peak broadening is due to inhomogeneous strain but can also be due to a change in particle size (or morphology). As is known from powder diffraction, peak width is

linearly proportional to strain and inversely proportional to crystallite size [20]. The point that the width rises rapidly (+50 ps) also coincides with the a plateau in peak shift. This can be explained if the particle is undergoing some transient surface melting. The plateau is caused by the energy no longer going into heating the lattice but instead as latent heat of fusion to partially melt the particle. The rapid change in peak width commensurate with this supports this as the width can be interpreted as a reduction in particle size or a change in morphology. The transient nature of the partial melting is evident in the same behavior for later times. Further evidence for the transient melting can be seen in the significant softening of the longitudinal acoustic phonons which is shown in Fig. 2e. The low-angle, low-frequency component of the dispersion is obtained by time-Fourier transform of the data which for a cubic crystal can give the speed of sound from the gradient of scattering vector with frequency. The speed of sound for Au (111) is shown as the gradient of the pale blue line and clearly shows the softening at the highest fluence, with a reduction of $\approx 25\%$. Interestingly, partial quantinisation is evident in the dispersion curve (in both temporal and spatial directions) due to the finite size of the nanocrystal and the coherence of the X-rays. Figure 2 (f) shows partial line-outs for two angular frequencies as a function of scattering vector, highlighting the softening with increasing fluence. The straight line has been drawn as a visual aid (connecting the center of masses of the peaks) with its slope giving the speed of sound in the nanocrystal. We note the importance of being able to obtain such information on individual nano crystals, particularly related to heat transport in nano systems [22].

As the data were collected from a single nanocrystal using coherent X-rays with a geometry to allow sampling of the diffraction pattern greater than twice the Nyquist frequency, real-space

images could be obtained via iterative phase retrieval [15,16,23]. A phase retrieval algorithm was developed and employed to exploit the redundancy of the time resolved data (see supplementary methods). Shown in Fig. 3 are images of the projected density (a) and displacement (b) for the (111) Bragg peak (also see SI movies 2 and 3 respectively). The pertinent features of the nanocrystal is the small depression on the left hand edge. This absence of density can be interpreted as twinned region which does not satisfy the Bragg condition. The morphology of the crystal is well reproduced for the lowest fluence for all delay times. As the fluence is increased it is evident that the morphology and size of the nanocrystal changes dramatically. This change and partial restoration of the shape (with time) is indicative of a partial melting of the outer layer of the nanocrystal. This assertion is also corroborated by the time-dependent auto-correlation (Supplementary Figure. 1) whose boundary provides information on the size and any change in shape of the nanocrystal (Supplementary Methods) and is obtained directly from the data. To eliminate the possibility that the observed density changes are not in fact due to a shift along the third reciprocal space direction, simulations of the expected data and auto-correlation were calculated for the experimental conditions (including noise) and are shown in Supplementary Fig. 3. This demonstrates that even large shifts (compared to that observed) result in negligible changes compared to those observed. Figure 3 (b) shows that the deformation increases with increasing fluence as well as increasing at the delay times which show the largest peak shift and increase in width. A noticeable feature that is present in the highest fluence images is the corrugated appearance at the edges of the nanocrystal in the projected displacement. This could be attributed to a non-uniformity in the surface layer during melting with a quasi-periodic arrangement of liquid-like regions, supporting the hypothe-

ses if non-homogenous surface melting. The time-dependent density and deformation change is shown in Fig. 4 (a) and (b) respectively which is a slice through the center of the nanocrystal along $\boldsymbol{r}_{\parallel}$. For the highest fluence there is a clear retreat of the boundary (with delay time) of the nanocrystal with partial restoration of its extent. The time-frame for complete restoration is longer than the measurement time (500 ps after irradiation) and is consistent with other studies looking at ensemble melting [4]. The crystal does however achieve complete (within the resolution limits of the experiment) restoration of its shape and pertinent features since the highest fluence data was taken prior to the other fluences. The similarity of the negative delay times for all fluences demonstrates the complete reversibility of the process. The derivative of the deformation along the $\boldsymbol{r}_{\parallel}$ direction is shown and provides some information on the strain (we note this is not the actual strain but we use this as a proxy for the strain). The periodic deformation is evident in the 'strain' with some asymmetry present and its subsequent departure from harmonicicty at the highest fluence. The largest strain is 0.3% which is significantly below the bulk strain expected before melting [4].

We have been able to observe transient melting in an individual nanocrystal using an XFEL in a 'pump-probe' experiment. We have been able to verify and confirm several outstanding details regarding this phenomenon. Primarily, that partial melting occurs, in a non-homogenous fashion with complete restoration of the morphology. The surface melting occurs at lower temperatures than bulk melting. We have also shown that it is possible to obtain low-frequency and -wave-vector acoustic phonons from an individual nano-crystal and observed their subsequent softening as transient melting occurs. The results and techniques demonstrated here provide significant insight into phase transitions and dynamics in nano particles and will find application in many

other areas.

Methods Summary

Sample preparation. A 2 nm layer of titanium was deposited using thermal evaporation onto an silicon wafer followed by 20 nm of gold. The thin film was then annealed in air at 1000°C for approximately 10 hours after which time the film had dewetted and formed nanocrystals.

Experiment. The experiment was performed at the XPP instrument at the LCLS. A 1520×1520 pixel CS-PAD with 110 μm square pixels was used to record the diffraction. The Beryllium lenses were positioned so that the sample position was out of the nominal focus. This regime was chosen so that the X-ray pulses from the LCLS did not destroy the sample. Damage from either the optical or X-ray pulses was monitored using a confocal microscope (Olympus LEXT) mounted directly above the sample. To record the 3D diffraction pattern, the nanocrystals were rocked in 41 0.02° steps. At each position, 1000 diffraction patterns were recorded. Filtering of the data was done *ex post facto* to remove saturated frames and blank shots, with the final summed patterns consisting of the 100 brightest, non-saturated shots (see Supplementary Information). These data were subsequently inverted using a phase retrieval algorithm (see Supplementary methods) to obtain real-space images of electron density and projected displacement.

1. Jurgilaitis, A. *et al.* Time-resolved x-ray diffraction investigation of the

modified phonon dispersion in insb nanowires. *Nano Letters* **0**, null (0). URL http://pubs.acs.org/doi/abs/10.1021/nl403596b. http://pubs.acs.org/doi/pdf/10.1021/nl403596b.

2. Wang, N., Rokhlin, S. I. & Farson, D. F. Nonhomogeneous surface premelting of au nanoparticles. *Nanotechnology* **19**, 415701 (2008). URL http://stacks.iop.org/0957-4484/19/i=41/a=415701.

3. Hartland, G. V., Hu, M., Dame, N. & Sader, J. E. Softening of the Symmetric Breathing Mode in Gold Particles by Laser-Induced Heating 7472–7478 (2003).

4. Plech, a., Kotaidis, V., Grésillon, S., Dahmen, C. & von Plessen, G. Laser-induced heating and melting of gold nanoparticles studied by time-resolved x-ray scattering. *Physical Review B* **70**, 1–7 (2004). URL http://link.aps.org/doi/10.1103/PhysRevB.70.195423.

5. Plech, A. *et al.* LETTERS A Surface Phase Transition of Supported Gold Nanoparticles (2007).

6. Ruan, C.-Y., Murooka, Y., Raman, R. K. & Murdick, R. A. Dynamics of size-selected gold nanoparticles studied by ultrafast electron nanocrystallography. *Nano Letters* **7**, 1290–1296 (2007). URL http://pubs.acs.org/doi/abs/10.1021/nl070269h. http://pubs.acs.org/doi/pdf/10.1021/nl070269h.

7. Perner, M. *et al.* Observation of hot-electron pressure in the vibration dynamics of metal nanoparticles. *Physical Review Letters* **85**, 792–795 (2000). URL http://link.aps.org/doi/10.1103/PhysRevLett.85.792.

8. Kim, W. *et al.* Thermal conductivity reduction and thermoelectric figure of merit increase by embedding nanoparticles in crystalline semiconductors. *Phys. Rev. Lett.* **96**, 045901 (2006). URL http://link.aps.org/doi/10.1103/PhysRevLett.96.045901.

9. Wang, X. *et al.* Noninvasive laser-induced photoacoustic tomography for structural and functional in vivo imaging of the brain. *Nat Biotech* **21**, 803–806 (2003). URL http://dx.doi.org/10.1038/nbt839.

10. Gobin, A. M. *et al.* Near-infrared resonant nanoshells for combined optical imaging and photothermal cancer therapy. *Nano Letters* **7**, 1929–1934 (2007). URL http://pubs.acs.org/doi/abs/10.1021/nl070610y. http://pubs.acs.org/doi/pdf/10.1021/nl070610y.

11. Yang, Y.-Y. *et al.* High-harmonic and single attosecond pulse generation using plasmonic field enhancement in ordered arrays of gold nanoparticles with chirped laser pulses. *Opt. Express* **21**, 2195–2205 (2013). URL http://www.opticsexpress.org/abstract.cfm?URI=oe-21-2-2195.

12. Peters, K. F., Cohen, J. B. & Chung, Y.-W. Melting of pb nanocrystals. *Physical Review B* **57**, 13430–13438 (1998). URL http://link.aps.org/doi/10.1103/PhysRevB.57.13430.

13. Wang, N., Rokhlin, S. I. & Farson, D. F. Ultrafast laser melting of au nanoparticles: atomistic simulations **13**, 4491–4509 (2011). URL http://dx.doi.org/10.1007/s11051-011-0402-3.

14. Gan, Y. & Jiang, S. Ultrafast laser-induced premelting and structural transformation of gold nanorod. *Journal of Applied Physics* **113**, 073507 (2013). URL http://link.aip.org/link/?JAP/113/073507/1.

15. Clark, J. N. *et al.* Ultrafast three-dimensional imaging of lattice dynamics in individual gold nanocrystals. *Science* **341**, 56–59 (2013). URL http://www.sciencemag.org/content/341/6141/56.abstract. http://www.sciencemag.org/content/341/6141/56.full.pdf.

16. Pfeifer, M. A., Williams, G. J., Vartanyants, I. A., Harder, R. & Robinson, I. K. Three-dimensional mapping of a deformation field inside a nanocrystal. *Nature* **442**, 63–66 (2006).

17. Trigo, M. *et al.* Fourier-transform inelastic x-ray scattering from time- and momentum-dependent phonon-phonon correlations. *Nat Phys* **9**, 790–794 (2013). URL http://dx.doi.org/10.1038/nphys2788.

18. EmmaP. *et al.* First lasing and operation of an angstrom-wavelength free-electron laser. *Nat Photon* **4**, 641–647 (2010). URL http://dx.doi.org/10.1038/nphoton.2010.176.

19. Hart, P. *et al.* The cspad megapixel x-ray camera at lcls 85040C–85040C–11 (2012). URL + http://dx.doi.org/10.1117/12.930924.

20. Williamson, G. & Hall, W. X-ray line broadening from filed aluminium and wolfram. *Acta Metallurgica* **1**, 22 – 31 (1953). URL http://www.sciencedirect.com/science/article/pii/0001616053900066.

21. Thomsen, C., Grahn, H. T., Maris, H. J. & Tauc, J. Surface generation and detection of phonons by picosecond light pulses. *Phys. Rev. B* **34**, 4129–4138 (1986).

22. Cahill, D. G. *et al.* Nanoscale thermal transport. ii. 2003–2012. *Applied Physics Reviews* **1**, – (2014). URL http://scitation.aip.org/content/aip/journal/apr2/1/1/10.1063/1.4832615.

23. Fienup, J. R. Phase retrieval algorithms - a comparison. *Appl. Opt.* **21**, 2758–2769 (1982).

Acknowledgements This work was supported by FP7 advanced grant from the European Research Council. A.H. was supported by AWE. J.S.W. is grateful for support from the UK EPSRC under grant no. EP/H035877/1. The experimental work was carried out at the Linac Coherent Light Source, a National User Facility operated by Stanford University on behalf of the US Department of Energy, Office of Basic Energy Sciences.

Additional information Reprints and permissions information is available at www.nature.com/reprints. The authors declare no competing financial interests. Correspondence and requests for materials should be addressed to J.N.C. (email: jesclark@stanford.edu) or I.K.R (email: i.robinson@ucl.ac.uk).

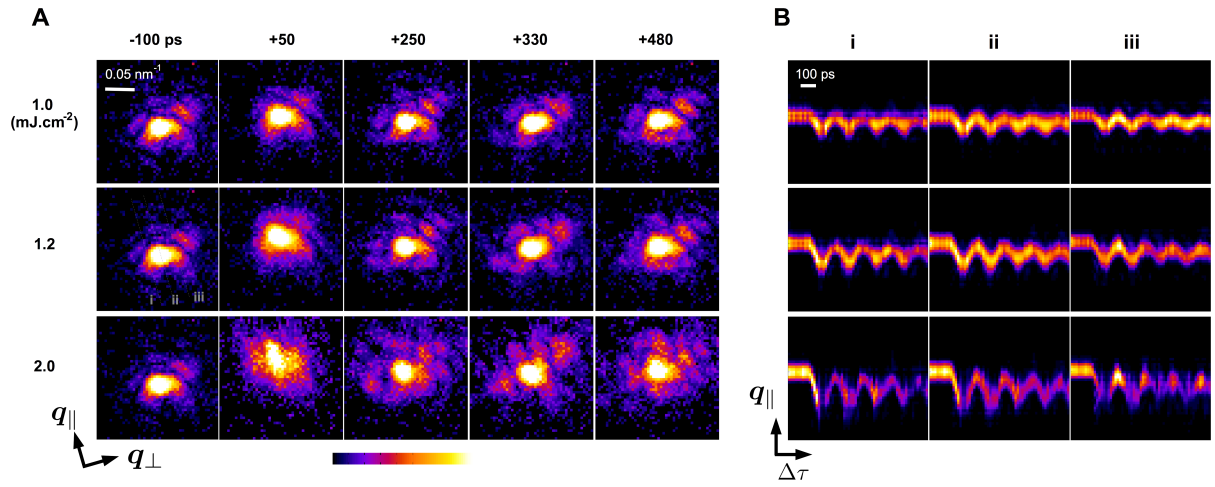

Figure 1: **Selected diffraction data from a single nanocrystal.** Diffraction from a single gold nanocrystal as a function of pump-laser fluence (vertical) and pump-probe delay time (horizontal). Significant non-linear broadening of the peak occurs at the highest fluence for selected times. $\boldsymbol{q}_{\|}$ points in the direction of the gold (111) scattering vector.

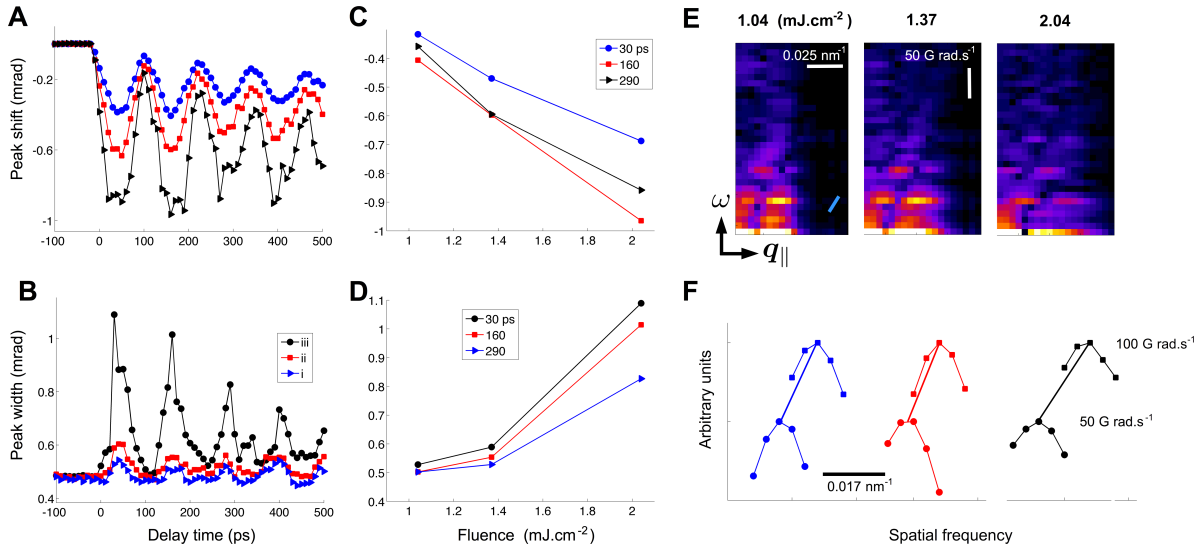

Figure 2: **Time-dependent peak position and width for a single nanocrystal .** a) The center of mass and (b) peak width as a function of delay time for the three different fluences. Non-linear peak shift and peak brooding can be observed for select times in (c) and (d) respectively. The non-linear peak shift can be attributed to partial melting of the surface with the subsequent size change resulting in a non-linear broadening.

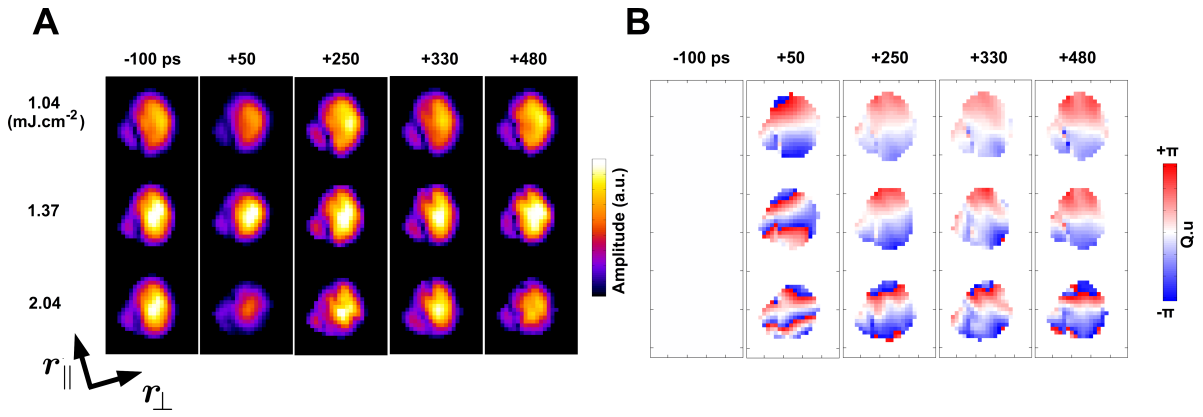

Figure 3: **Real-space images of a nanocrystal undergoing transient melting** a) Recovered real-space images for selected times (horizontally) and as a function of fluence (vertically). Significant morphology changes are apparent for the highest fluence, consistent with a loss of crystallinity attributed to surface melting. The most dramatic changes occur at the point where the greatest non-linearity occurs (+50 ps). b) Recovered images of the phase (modulo 2π or 1 lattice spacing) after subtraction of the -100 ps time. The phase shows the projected displacement as a function of time (horizontally) and fluence (vertically).

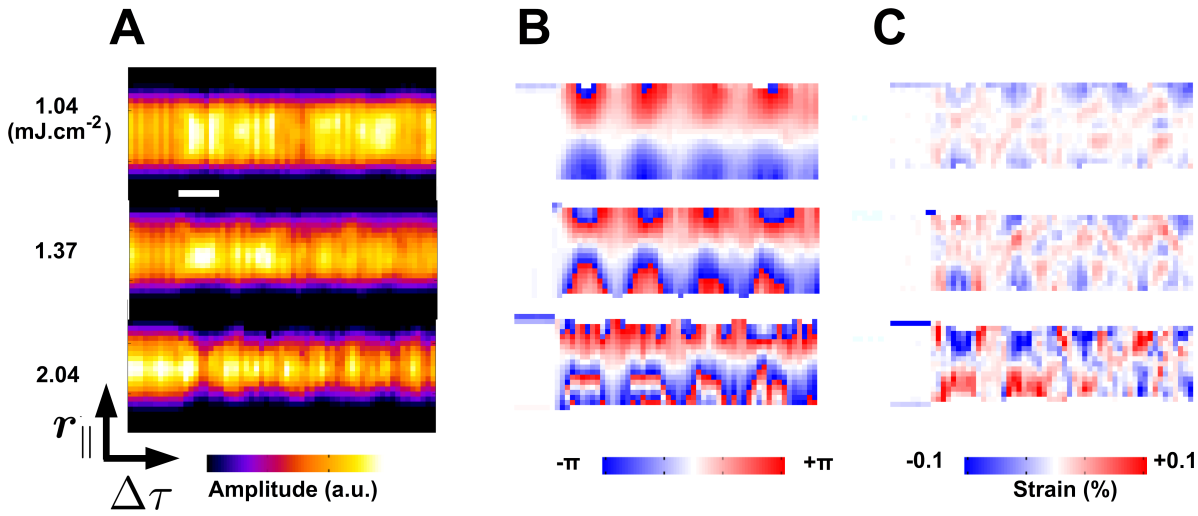

Figure 4: **Time-dependent density, displacement and strain** a) The time dependent density shown as a central slice through the nanocrystal for the three fluences parallel to the direction of the (111) scattering direction. It is evident at the highest fluence that there is a morphology and size change. b) The recovered phase shows the deformation through a projection of the displacement field (after subtraction of the initial phase). The magnitude of the deformation grows with the fluence and the harmonic behavior begins to depart. c) The 'strain' in the (111) direction is shown, taken from the derivative along the (111) direction. The largest excursions of the Bragg peak coincide with the largest values of the strain.